J. Fluid Mech. (1984), *vol.* 144, *pp.* 153–176
Printed in Great Britain

Study of the effects of wall conductance on natural convection in differently oriented square cavities

By D. M. KIM AND R. VISKANTA
School of Mechanical Engineering, Purdue University, West Lafayette, IN 47907

(Received 11 October 1983)

This paper reports experimental and numerical results on the effects of wall conductance on natural convection in a two-dimensional rectangular cavity. Three different configurations in which the external wall is heated from the side, top and bottom and cooled from the side, bottom and top respectively have been investigated. Experiments have been performed in a square enclosure with solid walls made from Lexan and forming a square air-filled cavity. A Mach–Zehnder interferometer was used to determine the temperature distributions in the fluid. Solutions for stationary two-dimensional equations of energy and motion governing heat conduction in the solid and natural convection flow and heat transfer of a Boussinesq fluid contained in the cavity have been obtained numerically. The coupled flow distributions, including the appearance of multicellular flow, temperature profiles and heat-transfer predictions compare favourably with experimental results. Heat conduction in the connecting (unheated) walls is shown to simultaneously stabilize and destabilize the fluid in the cavity.

1. Introduction

Natural-convection heat transfer in cavities has been receiving considerable attention. Numerous experimental and numerical computational studies dealing with natural convection in enclosures have been reported in the literature. Excellent reviews are available (Catton 1978; Ostrach 1982; Catton *et al.* 1983) and there is no need to repeat them. Most of the studies have neglected the interaction between convection in the fluid-filled cavity and conduction of heat in the walls forming the enclosure by using idealized boundary conditions such as those corresponding to a prescribed temperature or heat flux. In all enclosures thermal boundary conditions (wall conductance) can lead to stabilization or destabilization of the flow and corresponding large changes in the convective heat-transfer coefficient. Heat conduction in insulated (on the outside) walls forming a cavity causes the temperature distribution in the insulated wall to deviate from that of the adiabatic case, and thus precludes the possibility of obtaining experimentally a truly adiabatic boundary condition in some fluids such as air. Natural convection in the cavity can also induce conduction heat transfer in the surrounding walls (ElSherbiny, Hollands & Raithby 1982). The major thesis of this paper is that wall heat conduction and radiation interchange among the walls are inevitable in any cavity.

It has been recognized for some time that thermal boundary conditions (wall conductance and radiation heat-exchange) on enclosure boundaries influence convective flow and heat transfer, but relatively little work has been done (Catton *et al.* 1983). Solutions have been obtained for the case when the unheated walls of the enclosure are adiabatic and perfectly conducting (Catton, Ayyaswamy & Clever 1974). The results show large differences in the local convective heat transfer at the heated wall for the two cases, particularly in the vicinity of the unheated wall. Natural convection in a two-dimensional enclosure surrounded by one-dimensional conducting and radiating walls has been studied numerically (Larson & Viskanta 1976). The effects of cell-wall thickness and thermal conductivity on natural-convection heat transfer within inclined rectangular cavities have been analysed in order to gain understanding of the efficiency of cellular structures to reduce convective heat losses in flat-plate solar collectors (Koutsoheras & Charters 1977; Meyer, Mitchell & El-Wakil 1982). Natural convection in a rectangular enclosure subjected to comparable horizontal and vertical temperature differences has been studied (Shiralkar & Tien 1982). No experimental studies of the problem considered in the paper have been identified in the literature, but two recent, remotely related experiments should be mentioned (Meyer *et al.* 1982; Krane & Jesse 1983). The effects of thermal boundary conditions on buoyancy driven convective flow in cavities has been identified as an important problem for future research (Catton *et al.* 1983).

The intent of this present study is to investigate experimentally and analytically the effects of wall heat conduction on natural convection in a two-dimensional square cavity having finite wall conductances in which air was used as the working fluid. Three different orientations of the heated enclosure wall with respect to the gravitational field are considered: (i) heating from a vertical wall and cooling from the opposite side; (ii) heating from the top and cooling from the bottom; and (iii) heating from the bottom and cooling from the top. Experimental data were obtained for a square enclosure made of relatively low thermal conductivity material with atmospheric air as the working fluid in the cavity. To obtain improved understanding of the effects of wall conductance on the convective flow, data are compared with the numerical results based on a theoretical model.

2. Experiments

The purpose of the experiments was to simulate in a well-controlled laboratory experiment convective heat transfer in a cavity surrounded by finite-conductance walls and to gain understanding of the effects of heat conduction in the walls on natural convection in the fluid. To this end, three different orientations of the heated–cooled surfaces with respect to the gravitational field have been studied (figure 1). In the experiments the emphasis is on the convective effects resulting from heat conduction in the walls and from the system orientation.

2.1. *Test cell*

A schematic diagram of the test cell used for the experiments is shown in figure 2. Because of the symmetry in the geometry and boundary conditions of the test material, the test cell is formed by combining three identical rectangular structures. The central part of the test solid was used for the measurement, and the two sides of the test material served to minimize edge effects, such as heat gains or losses, by the test material. The inside dimensions of each cavity test material are 3.6 by 3.6 cm and the outside dimensions are 6 by 6 cm. The length of a test cell along the optical path is 19 cm. A larger test cell would have been desirable to minimize the edge effects. Unfortunately, a width and height limit in the direction of the optical path is imposed by the available interferometer optics. A Mach–Zehnder interferometer of typical rectangular design having 25 cm diameter optics was employed as a diagnostic tool for measuring the temperature distribution in a cavity filled with air at atmospheric

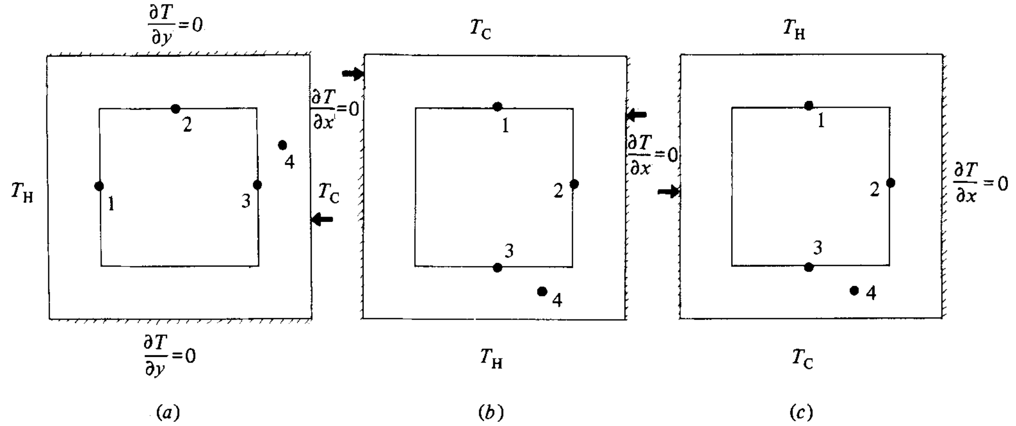

FIGURE 1. Three different orientations of the test conditions and thermocouple locations for the measurement in the solid wall: (*a*) side heating; (*b*) bottom heating; (*c*) top heating.

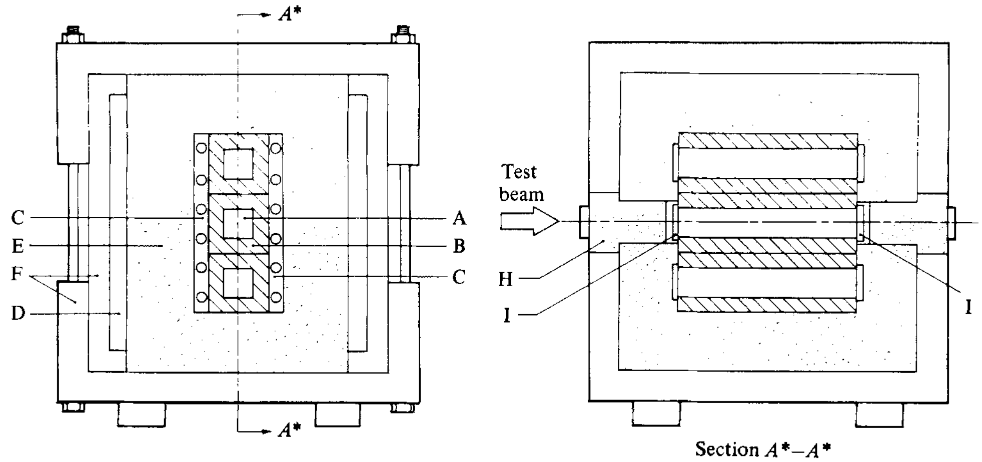

FIGURE 2. Test cell: A, test region (air); B, test region (solid); C, heat exchanger; D, air gap; E, insulation materials; F, flanges; G, optical glass; H, removable door.

pressure. The entire test cell was designed so that it could be easily oriented, and the three heating conditions illustrated in figure 1 (i.e. heating from the side and cooling from the side, heating from the bottom and cooling from the top, and heating from the top and cooling from the bottom) could be investigated.

Lexan was chosen as the wall material because it is readily machinable, has low thermal conductivity, has well-established thermophysical properties and is moderate in cost. A moderate Biot number is required in order to investigate conduction-induced or stabilized convection in a cavity. If the thermal conductivity is too high, the Biot number becomes too small and conduction becomes the dominant heat-transfer mode in the system. This is one of the most important reasons why Lexan was chosen as a test material instead of others. The thermophysical properties of Lexan at a temperature of 25 °C are as follows (Stedfeld 1979):

$$\begin{aligned}\text{Thermal conductivity} &= 0.201\ \mathrm{W\ m^{-1}\ {}^{\circ}C^{-1}},\\ \text{Specific heat} &= 1256.0\ \mathrm{W\ s\ kg^{-1}\ {}^{\circ}C^{-1}},\\ \text{Specific gravity} &= 1.2.\end{aligned}$$

The interior surface of the cavity was carefully sprayed with several coats of 3M Nextell Black Velvet paint to give the surface an emissivity greater than 0.99.

Two of the outside walls of the test cell were maintained at uniform but different temperatures. Multiple-pass heat exchangers, through which a working fluid at a desired temperature can be circulated by a constant-temperature bath and maintain the surfaces at a uniform temperature, were designed and attached to the walls of the test cell to provide constant-temperature boundaries. Optical-quality glass windows, with dimensions 4.0 by 4.0 and 0.9 cm thick, were installed at the front and back faces of the test cell for interferometric measurements. The entire test cell (top, bottom, sidewalls and ends) were covered by two layers (10 cm thick) of Styrofoam insulation in order to minimize heat gains or losses from the surroundings. The ends of the test cell were covered with removable insulation to facilitate photographic and optical observations.

The thermal boundary conditions imposed on the outside walls of the test cell were established by circulating a temperature-controlled working fluid from a constant-temperature bath. Two temperature baths were used in the experiments. This temperature bath was capable of maintaining a present temperature to within 0.1 °C at a maximum flow rate (4.0 litre/min).

2.2. *Instrumentation*

Eleven copper–constantan thermocouples were used for measuring temperatures at different locations in the solid. All of the thermocouples were placed at the centre of the midplane of the solid. They were read with an automatic-scanning multichannel data logger with a printer capable of resolving 0.1 °C and a calibrated accuracy of 0.1 °C.

The temperature distribution in the fluid (air) filling the cavity was measured using a Mach–Zehnder interferometer. A 10 mW He–Ne laser served as the light source for the interferometer, The primary reason for using a laser source was that it eliminated the need for compensation of the optical path in the reference leg of the interferometer.

2.3. *Test procedure and data reduction*

The test cell was fixed in the test position and centred in the test beam of the interferometer. A 35 mm camera was used to photograph the interference-fringe pattern reflected from the parabolic mirror and focused at the centre of the test cell. Kodak technical film (TP 135–36) was used to obtain clear and sharp photographs of the interference-fringe images.

The test was initiated by supplying the heat exchanger with a working fluid to impose isothermal boundary conditions on the outside walls of the cell. A photograph of the interference-fringe patterns was taken every ten minutes by removing the insulation covering the windows to facilitate photographing of the patterns. The insulation was immediately replaced after photographing. At the same time, the temperatures in the solid were recorded using the data logger. The experiments continued until steady-state conditions were reached. A steady state was assumed to exist when the temperatures at the solid–fluid interface did not change.

The interference-fringe data were interpreted using the procedure described in the literature (Hauf & Grigull 1970). The temperature at a reference point was measured with a thermocouple. Then, for each reference fringe pattern evaluated, the fringe shifts were calculated for the temperature about the reference temperature. For a more convenient and accurate reduction of data, a computer program was written to determine the temperature at every fringe shift for the measured reference temperature.

3. Analysis

3.1. *Physical model and assumptions*

The physical model and coordinate system of the problem are illustrated schematically in figure 3. The two-dimensional rectangular cavity is formed by walls having finite conductance. The vertical and the horizontal walls can be of different thickness, but are assumed to be of the same material. Initially, the walls of the enclosure and the fluid inside the cavity are assumed to be at a constant, uniform temperature, and the fluid is taken to be stagnant. The horizontal connecting walls are assumed to be insulated on the outside. At time $t > 0$ constant but different temperatures are suddenly imposed on the outside of the two walls and maintained until steady-state conditions are reached.

It is assumed in the analysis that the thermophysical properties of the walls and of the fluid are independent of temperature, and the flow is laminar. The fluid is Newtonian, incompressible, and the Boussinesq approximation is valid. The fluid motion and heat transfer in the cavity are assumed to be two-dimensional. Radiation heat exchange between the walls is neglected in comparison with convection, and the fluid is assumed to be radiatively non-participating. Viscous heat dissipation in the fluid is assumed to be negligible in comparison with conduction and convection.

3.2. *Model equations*

For the sake of brevity, the conservation equations are written in dimensionless form from the start, but are given here only for the orientation when heating is from one vertical side and cooling is from the opposite one (see figure 1*a*).

The transient heat-conduction equation in the wall is

$$\frac{\partial \Theta_{\mathrm{w}}}{\partial \tau} = \alpha^{*}\left(\frac{l}{L}\right)^{2}\left[\frac{\partial^{2}\Theta_{\mathrm{w}}}{\partial \xi_{\mathrm{w}}^{2}} + \left(\frac{L}{H}\right)^{2}\frac{\partial^{2}\Theta_{\mathrm{w}}}{\partial \eta_{\mathrm{w}}^{2}}\right], \tag{1}$$

where

$$\Theta_{\mathrm{w}} = \frac{T_{\mathrm{w}} - T_{\mathrm{C}}}{T_{\mathrm{H}} - T_{\mathrm{C}}}, \quad \tau = \frac{\alpha t}{l^{2}}, \quad \xi = \frac{x}{l}, \quad \eta = \frac{y}{h},$$

$$\alpha = \frac{\kappa}{\rho c_{p}}, \quad \alpha^{*} = \frac{\alpha_{\mathrm{w}}}{\alpha}.$$

The conservation equations of mass, momentum and energy for the fluid can be expressed in standard form by introducing the concepts of stream function and vorticity. The dimensionless vorticity, energy and stream-function equations become respectively

$$\frac{\partial \Omega}{\partial \tau} + \left[\frac{\partial (U\Omega)}{\partial \xi} + \frac{1}{A}\frac{\partial (V\Omega)}{\partial \eta}\right] = Pr\left(\frac{\partial^{2}\Omega}{\partial \xi^{2}} + \frac{1}{A^{2}}\frac{\partial^{2}\Omega}{\partial \eta^{2}}\right) + Ra^{*}Pr\frac{\partial \Theta}{\partial \xi}, \tag{2}$$

$$\frac{\partial \Theta}{\partial \tau} + \frac{\partial (U\Theta)}{\partial \xi} + \frac{1}{A}\frac{\partial (V\Theta)}{\partial \eta} = \frac{\partial^{2}\Theta}{\partial \xi^{2}} + \frac{1}{A^{2}}\frac{\partial^{2}\Theta}{\partial \eta^{2}}, \tag{3}$$

$$\Omega = -\left[\frac{\partial^{2}\Psi}{\partial \xi^{2}} + \frac{1}{A^{2}}\frac{\partial^{2}\Psi}{\partial \eta^{2}}\right], \tag{4}$$

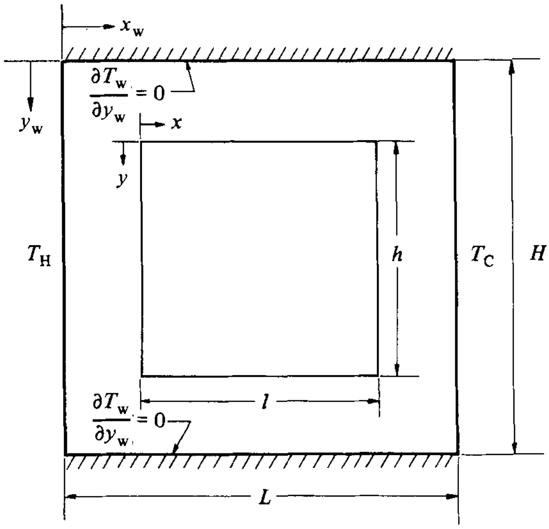

FIGURE 3. Physical model and coordinate system for heating from the left and cooling from the right vertical surfaces.

where

$$\Omega = \frac{\omega l}{U_0}, \quad U = \frac{u}{U_0}, \quad V = \frac{v}{U_0}, \quad \Theta = \frac{T-T_C}{T_H-T_C},$$

$$A = \frac{h}{l}, \quad Pr = \frac{\nu}{\alpha}, \quad Ra^* = \frac{g\beta(T_H-T_C)l^4}{\nu\alpha L}, \quad \Psi = \frac{\psi l}{U_0}.$$

The temperature boundary conditions on the outside walls of the enclosure are

$$\Theta_w(0, \eta_w, \tau_w) = 1, \tag{5}$$

$$\Theta_w(1, \eta_w, \tau) = 0 \tag{6}$$

and

$$\left.\frac{\partial \Theta_w}{\partial \eta_w}\right|_{\eta_w=0} = \left.\frac{\partial \Theta_w}{\partial \eta_w}\right|_{\eta_w=1} = 0. \tag{7}$$

The temperature boundary conditions at the interior walls (solid–fluid interface) of the enclosure are

$$\Theta_w(\xi, \eta, \tau)_w = \Theta(\xi, \eta, \tau)_w \tag{8}$$

and

$$\frac{\partial \Theta}{\partial \zeta} = k^* \frac{\partial \Theta_w}{\partial \zeta}, \tag{9}$$

where $k^* = k_w/k$. The boundary conditions on the velocity at the surface bounding the cavity are

$$U(\xi, \eta, \tau)_w = \Psi(\xi, \eta, \tau)_w = \frac{\partial \Psi}{\partial \eta}(\xi, \eta, \tau)_w = 0, \tag{10}$$

$$V(\xi, \eta, \tau)_w = \Psi(\xi, \eta, \tau)_w = \frac{\partial \Psi}{\partial \xi}(\xi, \eta, \tau)_w = 0. \tag{11}$$

The initial temperature and velocity boundary condition are taken as

$$\Theta_w(\xi,\eta,0) = \Theta(\xi,\eta,0) = \Theta_0(\xi,\eta,0), \tag{12}$$

$$U(\xi,\eta,0) = V(\xi,\eta,0) = 0, \tag{13}$$

$$\Omega(\xi,\eta,0) = 0. \tag{14}$$

We note that in addition to such customary dimensionless parameters as the Rayleigh number Ra, the Prandtl number Pr and the aspect ratio $A = h/l$ of the cavity, the following dimensionless groups arise: (i) the thermal diffusivity ratio α^*; (ii) the thermal conductivity ratio k^*; (iii) the aspect ratio H/L of the enclosure; and (iv) the void fraction ϕ. Even though they do not appear explicitly in dimensionless model equations, the arrangement of the cavity with respect to the wall and the void fraction ϕ are additional factors which influence the temperature distributions in wall and the fluid as well as the heat transfer across the system.

Analytical solutions of the model equations (1)–(4) are not feasible, and approximate methods available are not sufficiently flexible. Therefore a numerical solution procedure has been adopted. The ADI method (Peaceman & Rachford 1955) has been employed for the numerical solution of the system of transient elliptic equations. For this purpose the stream-function equation (4) was also rewritten in a transient form and solved using the ADI method until a steady state was reached. A non-uniform grid was used in the cavity to resolve the variables better near the boundaries. The details of the method of solution together with results verifying the numerical algorithm for the special case of isothermal walls are given elsewhere (Kim 1983). The accuracy of the numerical results obtained for the special case of isothermal vertical and perfectly adiabatic (horizontal connecting) walls was checked by comparing the predictions with the benchmark results (de Vahl Davis & Jones 1983) and good agreement has been obtained (Kim 1983). The results reported in this paper have been generated using a 26 × 26 grid for the enclosure and 16 × 16 in the cavity.

4. Results and discussion

A number of experiments have been performed for the three different orientations of the heated and cooled boundaries of the enclosure. The temperature differences imposed across the wall ranged from $\Delta T = 34$ °C to $\Delta T = 68$ °C. In all of the experiments the cold wall was maintained at a temperature of $T_C = -5$ °C. The maximum temperature in the test cell was limited by the material (Lexan) and heat-loss considerations. Owing to space limitations, only a representative sample of the large amount of available experimental data and numerical results are presented and discussed in this paper.

Before performing the experiments, an energy balance was established on the test cell. The details are given elsewhere (Kim 1983). Suffice it only to mention that the energy balance on the system was closed to within about 1.5 %. At larger temperature differences, the measured and predicted heat losses agreed with each other to within less than 1 % and accounted for about 7 % of the total energy input to the system.

4.1. *Heating and cooling from the sides*

Interference-fringe patterns

The interference fringe patterns in the fluid (air) photographed are given at different times in figure 4 for a particular experiment. Initially, the solid and the

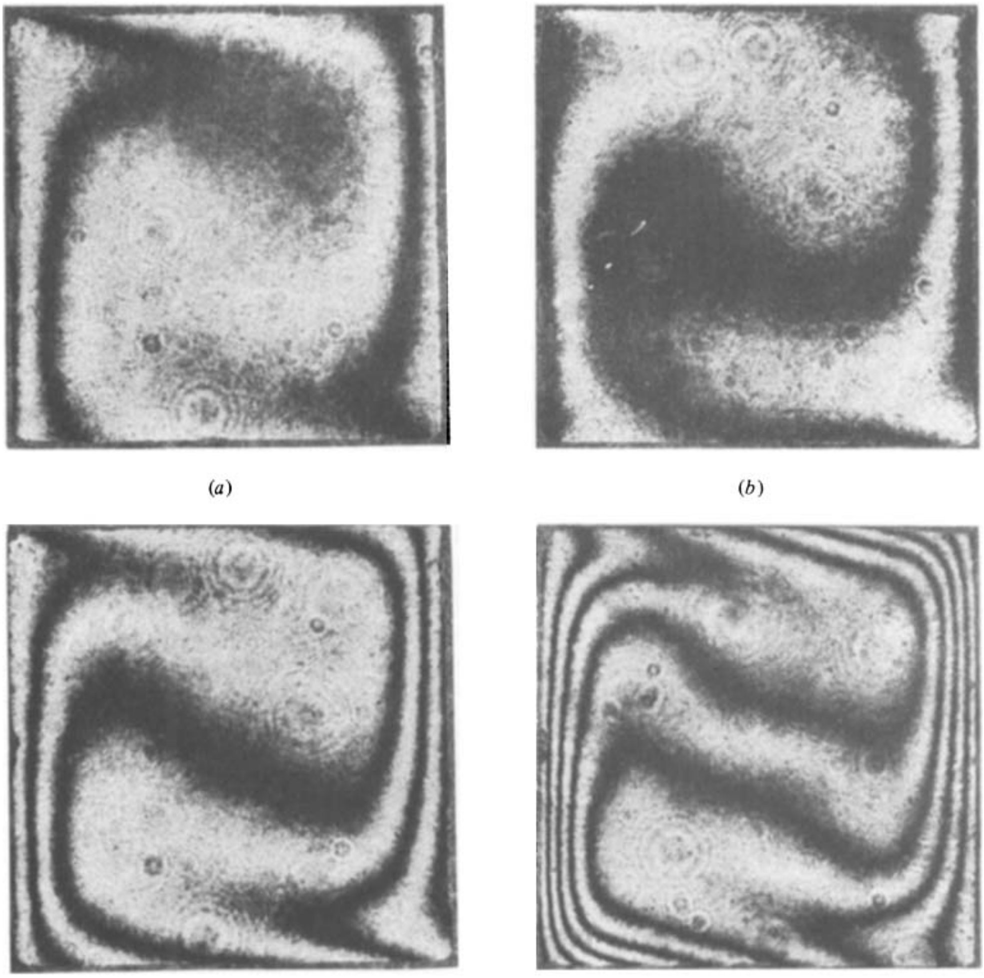

(a) (b)

(c) (d)

FIGURE 4. Transient isotherms for $Ra^* = 1.01 \times 10^6$, $A = 1$, $H/L = 1$, $\phi = 0.36$, $k^* = 7.4$, $Pr = 0.71$ and $\alpha^* = 0.008$: (a) $\tau = 5$; (b) 10; (c) 20; (d) ∞ (steady state).

fluid were at a uniform temperature $T_0 = 21$ °C ($\Theta_0 = 0.5$). The hot wall was kept at a temperature of $T_{\mathrm{H}} = 47$ °C ($\Theta_{\mathrm{H}} = 1.0$) and the cold wall at a temperature of $T_{\mathrm{C}} = -5$ °C ($\Theta_{\mathrm{C}} = 0$). The interference fringes first appeared near the vertical walls, since the thermal disturbance through the wall reached the fluid at $\tau = 5$. As a result of the temperature difference between the vertical wall and the fluid, a buoyancy force was generated and natural-convection motion was initiated in the cavity as shown in figure 4(*a*). The influence of natural convection on the fringe patterns became evident when the time progressed, as shown in figures 4(*b*, *c*), since the fringes became more distorted near the centreline of the cavity. The fringes are more dense near the vertical walls at steady state (figure 4*d*). This means that temperature gradients became greater as natural convection developed and boundary layers were formed near the heated (cooled) walls. Note that the temperature gradients do not vanish at the horizontal top and bottom surfaces of the cavity. These gradients also increase as the heating continues. It is appropriate to mention that during preliminary experimentation the image of the enclosure and the fringe-shift patterns were carefully monitored on a frosted-glass screen placed between the test cell and the camera in order to detect motions in the fringe field which would indicate instabilities in the fluid. At no time during the transient and after steady-state conditions had been reached were instabilities detected. Also, no oscillatory convection with periodic or non-periodic flow structures were observed. This may be due to the fact that the threshold Rayleigh number for such convection was not exceeded in the experiments.

The photograph (figure 4*d*) clearly shows that thermal boundary layers are formed near the vertical walls. The interference fringes are spaced almost equally along the top and the bottom surfaces of the cavity owing to adiabatic conditions imposed on the outside horizontal walls. In other words, the horizontal wall tries to maintain a linear temperature distribution due to heat conduction in the wall. The temperature gradients clearly indicate that there is heat flow from the fluid to most parts of the upper connecting wall. This is due to the fact that as the fluid sweeps the hot vertical wall it becomes heated. As the warm fluid flows along the upper wall it continues to be heated for a short distance, but at some point along the horizontal wall the direction of heat flow is reversed and the fluid begins to release some of its energy to the wall. As the cool vertical wall is approached the direction of flow is reversed. The fluid then flows along the cold vertical wall and continues to give up some of its energy. The direction of flow is again reversed by the bottom horizontal wall. As the lower connecting wall is swept by the cold fluid, the direction of heat flow is still from the fluid to the wall; however, the direction of heat flow is reversed at some distance from the vertical cold wall. The density of fringes is higher near the lower half than the upper half of the left (hot) wall. This indicates that the local heat flux is greater at the lower half of the wall forming the cavity. The interference fringe patterns at the right (cold) vertical wall indicate a trend that is opposite to that at the left (hot) wall.

Predicted isotherms and flow fields

Figure 5 shows the contours of the isotherms, the streamlines and the velocity vectors for the modified Rayleigh number $Ra^* = 10^6$. The dimensionless constant-temperature lines in both the solid (wall) and the fluid are given for temperature difference $\Delta\Theta = 0.1$. The bounding surfaces of the fluid-filled cavity are indicated with dashed lines. Figure 5(*b*) shows the streamlines in the fluid (inscribed region). The contours of the stream function are not spaced equally but have been selected to illustrate salient features of the flow. Figure 5(*c*) depicts the dimensionless isotherms in the fluid with greater resolution than could be shown in figure 5(*a*). The dimensionless velocity vectors are given in figure 5(*d*). The arrows denote the direction and magnitude of the absolute-velocity vector at each grid point. Near the adiabatic horizontal outside walls the temperature decreases almost linearly with the distance from the hot (left) vertical wall to the cold (right) vertical wall (figure 5). However, natural convection causes the fluid in the cavity to take up a temperature profile that is different from the linear one. Note that the isotherms clearly indicate that the top and bottom walls of the cavity are nowhere adiabatic, and heat is transferred to or from the walls to the fluid.

The streamlines (figure 5*b*) and velocity vectors (figure 5*d*) clearly show that the velocity boundary-layer thickness on the hot wall increases in the same way as on the cold wall. The growth is different and is largely due to the change in the effect of buoyancy. As expected, the velocity boundary layers are thickest in the corners of the cavity, where the direction of flow is changed.

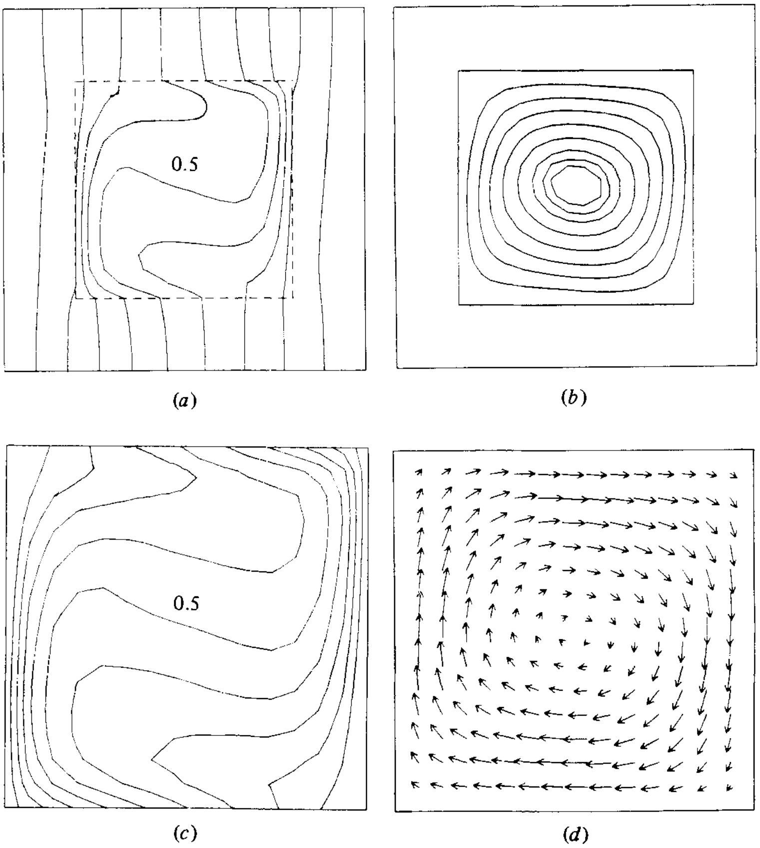

(a) (b) (c) (d)

FIGURE 5. The contours of (a) isotherms ($\Delta\Theta = 0.1$); (b) streamlines; (c) isotherms in the cavity ($\Delta\Theta = 0.065$); (d) velocity vectors. $Ra^* = 10^6$, $Pr = 0.71$, $A = 1$, $L/H = 1$, $\phi = 0.36$, $k^* = 10$ and $\alpha^* = 0.005$.

Extensive numerical results for a range of dimensionless parameters of interest have been obtained (Kim 1983), but cannot be reported here because of space limitations. For example, results show that as the Prandtl number is increased, the dimensionless velocities also increase, and natural-convection circulation becomes more intense.

Local and average Nusselt numbers

Because the rectangular cavity has four conducting walls, the local Nusselt number should be defined for all four walls. Figure 6 illustrates the local-Nusselt-number variations along the cavity walls. Because of the definitions adopted, the local Nusselt number is positive if heat flows from the wall to the fluid, and it is negative if heat flows from the fluid to the wall. At the connecting horizontal walls the local Nusselt number may be positive or negative, depending on the location along the walls. This indicates that for conjugate (combined conduction–convection) problems the Nusselt number may not be the most desirable heat-transfer parameter for correlating results and data. For the problem considered, the Nusselt number not only depends on the geometry of the cavity and the relevant conventional parameters (Ra^*, Pr and A), but also on the thermophysical properties of the wall materials, the porosity, and the orientation of the cavity within the solid wall.

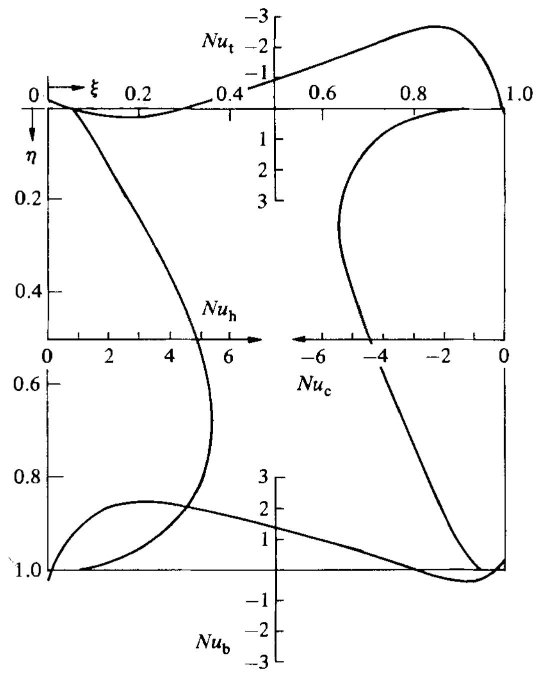

FIGURE 6. Local-Nusselt-number distributions along the four wallis; $Ra^* = 10^6$, $Pr = 0.71$, $A = 1$, $H/L = 1$, $\phi = 0.36$, $k^* = 10$ and $\alpha^* = 0.005$.

The maximum in the local Nusselt number at the hot inside (vertical) wall, Nu_h, occurs in the lower half of the cavity (figure 6). The results are consistent in trends with those reported in the literature (Bajorek & Lloyd 1982). As can be seen from the figure, the local Nusselt number attains the highest value near $\eta = 0.7$. This is caused by the cold fluid, which descended from the cold wall, moved along the lower surface, and impinged on the hot wall near its base. The location of the maximum local Nusselt number at the hot vertical wall is shifted down to the lower half of the cavity as the Rayleigh number is decreased. It is interesting to note the change in the heat-flow direction at the horizontal connecting walls. There is heat flow from the fluid to the wall and from the wall to the fluid at both the top and bottom of the horizontal connecting walls. The locations (along the horizontal walls) where the direction of heat flow is reversed depends on the Rayleigh number, the Prandtl number and other parameters (ϕ, A, L/H and k^*).

The local Nusselt number depends strongly on the void fraction of the solid wall. For example, the local Nusselt numbers with $\phi = 0.5$ are almost twice as large as those with $\phi = 0.25$ for the same Rayleigh number (Kim 1983). This is due to the larger temperature differences between the hot and the cold inside walls with an increase in the void fraction. It should be emphasized that the value of the Rayleigh number Ra^* is based on the outside wall temperature difference and the assumption of linear temperature variation across the system.

The results for the average Nusselt numbers have been calculated over a range of Rayleigh numbers and are presented in table 1. As the Rayleigh and Prandtl numbers increase, the average Nusselt number on the four walls of the cavity also increases. Although the average Nusselt numbers at the top and the bottom walls are quite small, the local Nusselt numbers can be quite large, as shown in figure 6. In

Pr \ Ra^*	10^4	10^5	10^6	10^7
0.01	1.176	1.291	2.130	3.300
0.1	1.252	1.661	3.092	4.580
0.71	1.310	2.195	3.801	5.517
10	1.329	2.303	4.154	5.957
100	3.180	3.325	4.312	6.262

TABLE 1. Effect of Prandtl number on the average Nusselt number at the hot vertical wall; $H/L = 1$, $\phi = 0.36$, $k^* = 10.0$ and $\alpha^* = 0.005$

other words, the total heat transfer across the top and bottom walls is small, since the average Nusselt number is quite small at the top and the bottom of the cavity, but the local heat transfer through the top and the bottom walls can be significant.

The results for the average Nusselt numbers at the hot wall have been calculated over a range of Rayleigh numbers, Prandtl numbers and void fractions. An empirical correlation of the average Nusselt number for a square cavity surrounded by conducting walls has been obtained from a least-squares fit of the numerical results:

$$\overline{Nu} = \begin{cases} 0.410\phi^{0.93}(k^*)^{0.138}(Ra^*)^{0.2} & (0.3 < Pr < 50), \qquad (15) \\ 0.485\phi^{0.93}(k^*)^{0.138}(Ra^*)^{0.2} & (50 < Pr < 100). \qquad (16) \end{cases}$$

These equations are based on the following range of parameters: $10^5 < Ra^* < 10^7$, $0.25 < \phi < 0.6$ and $3 < k^* < 100$. As both the Rayleigh number and the void fraction increase, the average Nusselt numbers on the hot wall of the cavity also increase.

It is desirable to compare the average Nusselt numbers given by (15) and (16) for an enclosure having finite-conductance walls with the results for enclosures with conducting or perfectly insulated horizontal connecting walls. The empirical correlations for the perfectly conducting and perfectly insulated horizontal walls reported in the literature (Roux *et al.* 1978) are

$$\overline{Nu} = \begin{cases} 0.13\,Ra^{0.28} & (10^4 < Ra < 10^5), \qquad (17) \\ 0.138\,Ra^{0.30} & (10^4 < Ra < 10^5), \qquad (18) \end{cases}$$

where $Ra = g\beta(T_H - T_C)\,l^3/\nu\alpha$. The average Nusselt number (with $Ra^* = 10^5$ and $k^* = 10$) calculated from (15) for a void fraction of 0.36 is 2.196, and for a void fraction of 0.5 it is 2.96. These two Nusselt numbers are compared with the average values of 3.27 and 4.44 which are obtained from (17) and (18) respectively, for a Rayleigh number of $Ra = 10^5$. The average Nusselt numbers for the two systems are not directly comparable, since the Rayleigh numbers are not based on the same temperature difference across the cavity.

As the thermal-conductivity ratio k^* increases, the average Nusselt number increases (Kim 1983). However, the value is not sensitive to the thermal-diffusivity ratio α^*. The effect of α^* should not be significant on the steady-state results, since the ratio is only important for transient conditions in the energy equation for the solid. The thermal-conductivity ratio k^* appears in the solid-fluid interface boundary conditions which control the solutions of the governing equations. Therefore the local

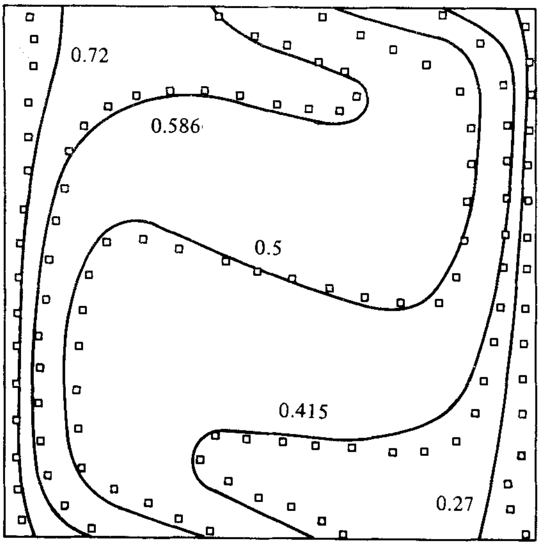

FIGURE 7. Comparison of the measured and predicted steady-state temperatures in air in the absence of radiation; $Ra^* = 0.64 \times 10^6$, $Pr = 0.71$, $A = 1$, $H/L = 1$, $\phi = 0.36$, $k^* = 7.4$ and $\alpha^* = 0.008$.

and the average Nusselt numbers are much more sensitive to the thermal-conductivity ratio than to the thermal-diffusivity ratio.

Comparison of predictions with experimental data

A rather critical comparison between the predicted and measured steady-state temperatures in air is shown in figure 7. The squares denote the experimental data points, and the solid lines denote the isotherms predicted by the model described in §3. The calculations presented here are based on a model that neglects radiation heat exchange among surfaces. The agreement between the analysis and the data is excellent throughout most of the cavity. One of the reasons for the good agreement is that radiation heat flux at the inside hot vertical wall is a relatively small fraction of the total (convective plus radiative) flux for the thermal conditions in the experiment (Kim 1983). The other factor contributing to the good agreement is that the temperature of the system is close to the ambient, so that heat losses (gains) to (from) the laboratory environment are very small in comparison to heat transfer across the system.

Figure 8 shows a comparison between the measured and predicted steady-state temperature distributions in the cavity for a larger temperature difference than for the experiment discussed in figure 7. Although the agreement between the data and predictions is good, the analysis could not predict accurately the data at the isotherms 0.21 and 0.79. The discrepancy between the data and predictions could be due to uncertainties in thermophysical properties of the solid and/or truncation error in the numerical model at higher modified Rayleigh numbers. Uncertainties in the knowledge of the vorticity boundary conditions at the solid–fluid interface and insufficiently fine grid for handling the nonlinearities of the variables at higher Rayleigh numbers may also contribute to this discrepancy. A comparison of the experimental data with model predictions when radiation heat exchange between surfaces is accounted for has been made (Kim 1983), but, for the sake of conciseness, the results are not given

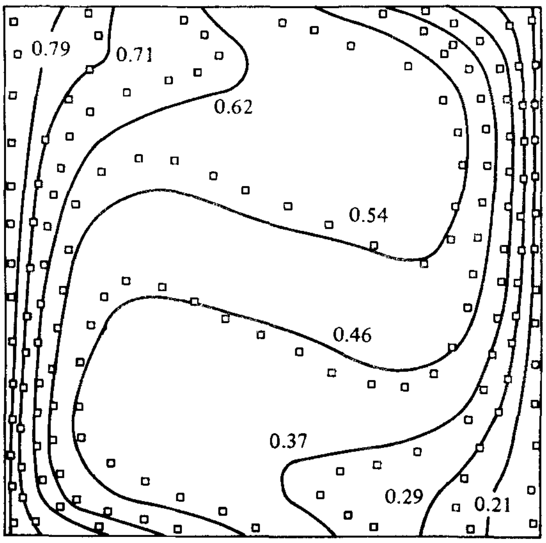

FIGURE 8. Comparison of the measured and predicted steady-state temperatures in air in the absence of radiation; $Ra^* = 1.01 \times 10^6$, $Pr = 0.71$, $A = 1$, $H/L = 1$, $\phi = 0.36$, $k^* = 7.4$ and $\alpha^* = 0.008$.

here. At higher temperatures and temperature differences imposed across the test wall the discrepancy between data and predictions increased because of the neglect of radiation heat exchange between the surfaces and increased heat losses from the test cell. The results show that inclusion of radiation exchange between surfaces for higher absolute temperatures of the system decreases the discrepancy between data and predictions at some locations and increases at the others (Kim 1983). The agreement between measured and predicted temperatures in the solid and the surface of the cavity was in general very good as the comparison is more forgiving than for the temperature distribution in the fluid.

The results (figures 7 and 8) show that the inside hot and cold surfaces of the cavity are not isothermal, but even more importantly, because of the finite conductance of the connecting horizontal walls, the surface temperatures of the connecting walls do not vary linearly with the distance as would be expected for perfectly adiabatic boundaries. The wall effects are clearly evident from an examination of the results. The interaction between conduction in the connecting horizontal walls and convection in the fluid produces unstable stratification of the fluid in the lower left- and the upper right-hand corners of the cavity. Density stratification results in the upper left- and lower right-hand corners of the cavity, and the stratification is more intense for the lower Rayleigh number (figure 7) than for the larger one (figure 8). This interaction causes relatively constant temperature regions adjacent to the heated and cooled walls respectively. The tendency toward thermal stratification causes an adverse temperatue gradient adjacent to the connecting walls, and this adverse temperature gradient appears likely to cause instability to secondary flow. However, such flow could not be detected from the interference-fringe patterns photographed.

For conjugate (combined conduction–convection) problems the Nusselt number may not be an appropriate parameter for correlating results, since it not only depends on the geometry of the cavity and the relevant parameters (Ra, Pr and A) but also on the thermophysical properties of the wall material, the porosity and the orientation of the cavity in the enclosure. Therefore local Nusselt numbers have not been

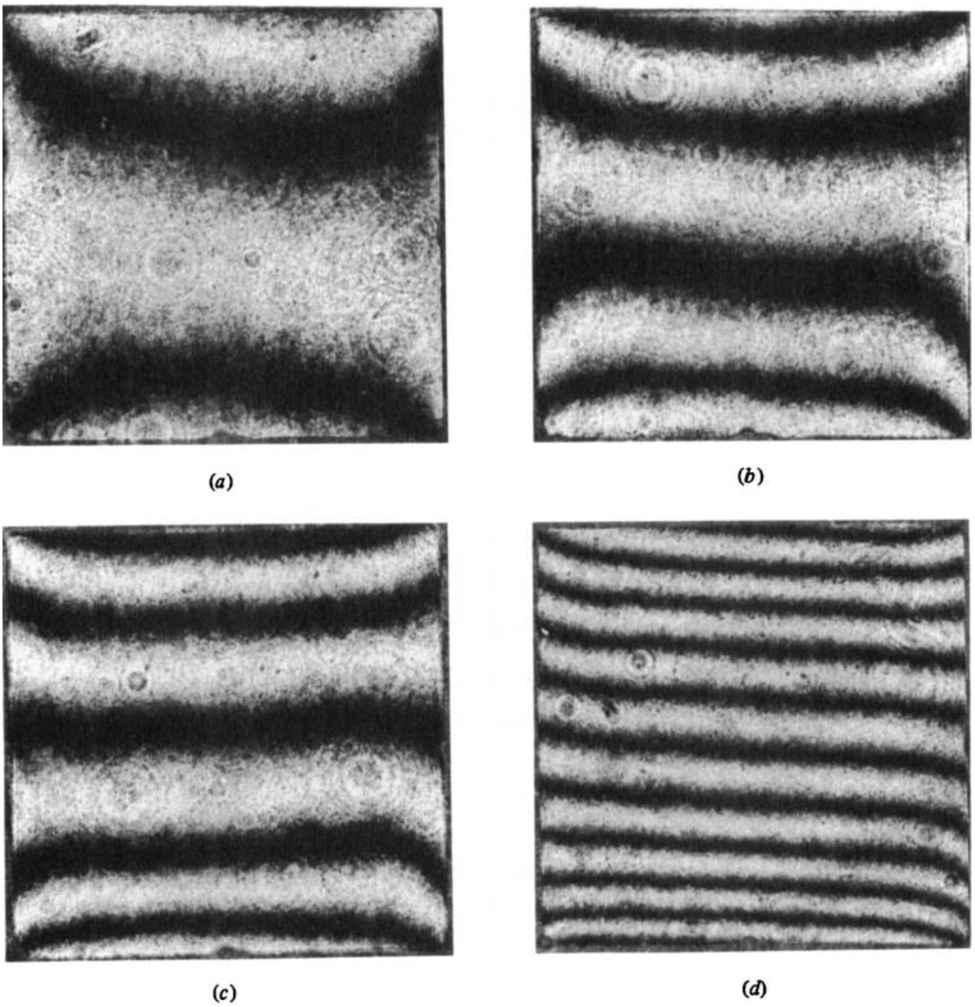
(*a*) (*b*) (*c*) (*d*)

FIGURE 9. Transient isotherms for $Ra^* = 1.01 \times 10^6$, $Pr = 0.71$, $A = 1$, $H/L = 1$, $\phi = 0.36$, $k^* = 7.4$ and $\alpha^* = 0.008$: (*a*) $\tau = 5$; (*b*) 10; (*c*) 20; (*d*) ∞ (steady state).

determined from interference-fringe data and compared with predictions, because there is a question of uniqueness. Since the local Nusselt number can become negative at the horizontal walls of the cavity, it appears that a local dimensionless heat flux may be a more suitable parameter for correlating the convective-heat-transfer results.

4.2. *Heating from the top and cooling from the bottom*

Interference-fringe patterns

The transient temperature distributions for heating the enclosure from above and cooling from below are shown in figure 9. The fluid is gravitationally stable, and heat flows only by conduction in the cavity. Initially, the solid and the fluid have a uniform temperature $T_0 = 21$ °C ($\Theta_0 = 0.5$). The hot wall is kept at a temperature of $T_H = 47$ °C ($\Theta_H = 1.0$), and the cold wall is maintained at a temperature of $T_C = -5$ °C ($\Theta_C = 0$). At early time the fringe patterns appear near the top and the

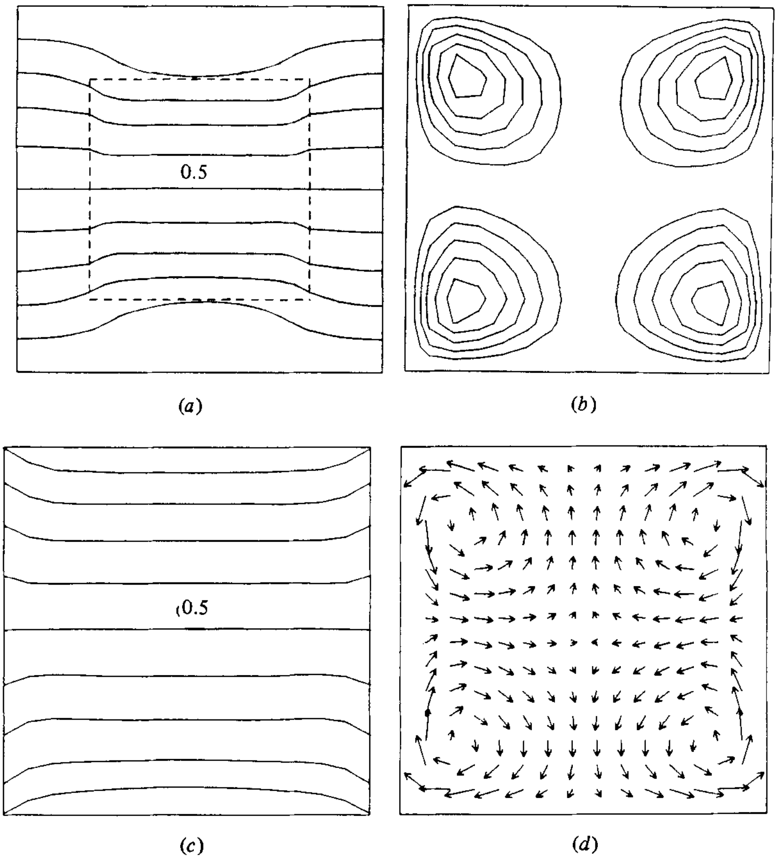

FIGURE 10. The contours of (*a*) isotherms ($\Delta\Theta = 0.1$); (*b*) streamlines; (*c*) isotherms in the cavity ($\Delta\Theta = 0.091$); (*d*) velocity vectors. $Ra^* = 1.01 \times 10^6$, $Pr = 0.71$, $A = 1$, $L/H = 1$, $\phi = 0.36$, $k^* = 7.4$ and $\alpha^* = 0.008$.

bottom of the cavity owing to the sudden thermal disturbance of the walls. As shown in figure 9(*a*), the isotherms are convex in shape at the top and the bottom of the cavity since the thermal diffusivity of air is larger than that of the solid ($\alpha/\alpha_w = 150$). As the time progresses, the number of fringes increases, but the fringes also straighten out along the horizontal plane, except near the vertical walls of the cavity. This is a result of thermal stratification of the fluids as shown in figures 9(*c*, *d*). In this configuration the heavier fluid lies below the lighter, and the fluid is always stable owing to higher temperatures at the top of the cavity. However, horizontal temperature gradients are produced at the solid–fluid interface owing to the differences in heat conduction between the solid and the fluid. The interference-fringe patterns photographed suggest that natural convection does indeed occur in the cavity where the buoyancy force is sufficiently large (i.e. near the vertical walls). However, this motion was probably relatively weak and was not detected using other independent means.

In a rectangular cavity heated from above the fluid should be stable and no convective motion could occur in the absence of heat conduction along the vertical walls. In the present experiment where the rectangular cavity is surrounded by conducting walls, the temperature difference between the solid and the fluid generates

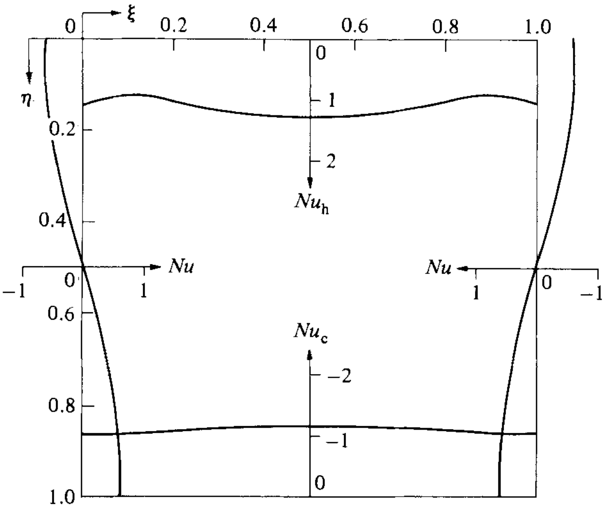

FIGURE 11. Nusselt number distributions along the four walls of the cavity (see figure 10 for parameters).

sufficiently large buoyancy force in the fluid and induces natural convection motion. As the temperature difference across the cavity increases, convective motions become more intense and increase mixing. The mixing produces a more uniform temperature (see figure 9*d*) along the horizontal plane. The interference-fringe patterns should be symmetric about the vertical plane through the centre of the cavity, but experimentally symmetry could not be realized. This is most likely due to non-symmetric heat losses to the ambient surroundings. The relatively large horizontal temperature gradients in the corners of the cavity indicate that convective transport of heat can be expected in the inherently stable orientation when the vertical walls have a finite conductance.

Predicted flow and temperature fields

Even though no detailed velocity measurements were made nor flow visualized, the predicted isotherms and velocity vectors (figure 10) provide useful information. Near the adiabatic vertical outside walls the temperature decreases almost linearly with the distance from the hot top wall to the cold bottom wall. However, differences in the thermal conductivities of the solid and the fluid produce a nonlinear temperature variation with the distance along the solid–air interface (figure 10*a*). As a result of nonlinear temperature gradients in the connecting vertical walls, convective motion is induced in the fluid. Four individual cells are formed in the cavity (figure 10*b*). The circulation produced in the cells is relatively weak because of thermal stratification of air in the cavity, but convective flows are consistent with the interference-fringe patterns photographed.

The steady-state local Nusselt numbers at the four walls of the cavity are shown in figure 11. In the absence of heat conduction along the vertical connecting walls, this is an inherently stable fluid configuration. A comparison of the results with those presented in figure 6 shows that the Nusselt numbers are considerably smaller for this arrangement, but they do not vanish at the connecting walls. The results also show that the Nusselt numbers at the hot and cold horizontal walls are not symmetric about the midplane of the cavity. At the connecting vertical walls, the Nusselt

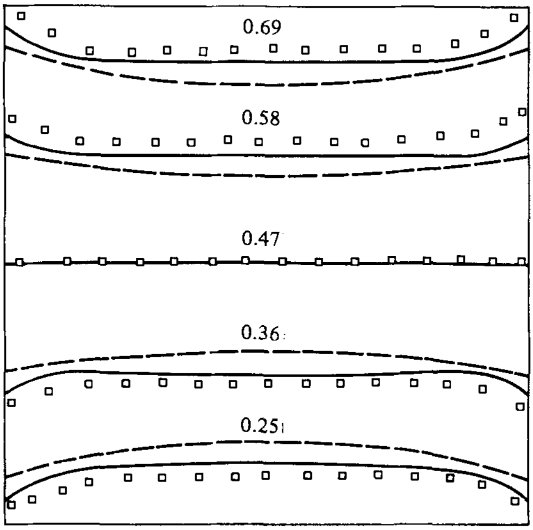

FIGURE 12. Comparison of the measured and predicted steady-state temperatures in air in the absence of radiation; $Ra^* = 0.64 \times 10^6$, $Pr = 0.71$, $A = 1$, $H/L = 1$, $\phi = 0.36$, $k^* = 7.4$ and $\alpha^* = 0.008$.

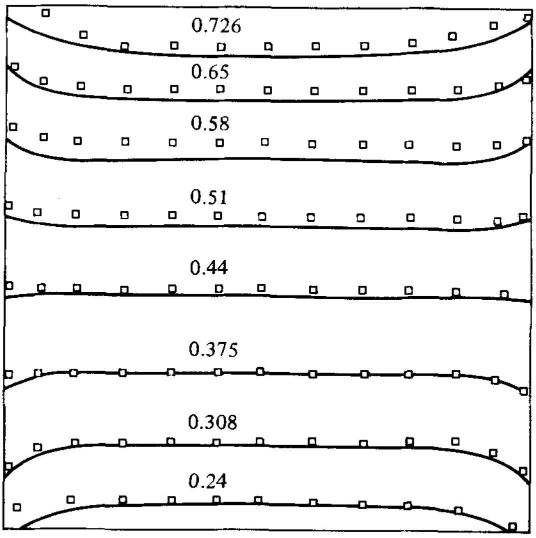

FIGURE 13. Comparison of the measured and predicted steady-state temperatures in air in the absence of radiation; $Ra^* = 1.01 \times 10^6$, $Pr = 0.71$, $A = 1$, $H/L = 1$, $\phi = 0.36$, $k^* = 7.4$ and $\alpha^* = 0.008$.

numbers change sign at the midplane of the cavity. They are negative in the upper half and positive in the lower half of the cavity.

Comparison of experimental data with predictions

A comparison between the measured and predicted steady-state temperatures in the cavity for one of the experiments is given in figure 12. The squares denote the experimental data and the solid lines represent numerical predictions. The agreement between the data and predictions is good throughout most of the cavity. In figure

12 the dashed lines indicate isotherms predicted by a pure-conduction model, i.e. absence of convection in air, and the solid lines denote the results with natural convection (solid lines) induced by heat conduction along the connecting vertical walls. Examination of results shows clearly that the model that considers convective motion in the fluid (solid lines) is in better agreement with the data than the one that considers conduction (dashed lines) in the fluid. The discrepancies could be due to uncertainties in the thermophysical properties of the solid and to the heat losses (gains) from the ends of the cells to the ambient surroundings. As mentioned previously, it should be remembered that the interference fringes represent temperatures averaged along the test beam, but the reference temperatue was obtained from the local surface temperature measured at the midplane of the test cell.

Figure 13 shows a comparison of steady-state measured and predicted temperatures in the cavity for a larger temperature difference than for the experiment discussed in figure 12. The agreement between the data and predictions is seen to be quite good. A comparison of measured and predicted temporal variation of temperature in the solid yielded excellent agreement (Kim 1983).

4.3. *Heating from the bottom and cooling from the top*

Interference-fringe patterns

The interference-fringe patterns were photographed during the transient and are presented for a typical experiment in figure 14. Initially, the solid and the fluid had a uniform constant temperature $T_0 = 21$ °C ($\Theta_0 = 0.5$). The hot wall was kept at a temperature of $T_H = 47$ °C ($\Theta_H = 1.0$), and the cold wall was maintained at a temperature of $T_C = -5$ °C ($\Theta_C = 0$). At $\tau = 5$ the fringes first appeared near the bottom and the top of the cavity owing to the penetration of the thermal wave through the wall. The effect of the buoyancy on the fringe appears to be small since the isotherms remain convex near the hot bottom at early times, as shown in figure 14(*a*). As the time progresses, the fringes move upward from the bottom and come down near the top of the cavity owing to the convective motion that has been established in the air. However, as evident from figure 14(*b*), most of the central core of the cavity remains at nearly uniform temperature. At steady state (figure 14*d*) the interference fringes are distorted and form cells. The flow may be 'turbulent' (random laminar flow) resulting from thermal-plume activity since the Rayleigh number reaches a value of the order of 10^6 (Chu & Goldstein 1973). However, owing to mixing the temperature in the central core of the cavity remains nearly uniform and cells are seen to form, as shown in figure 14(*d*). As the temperature difference across the wall increases, a more intense cellular motion develops, and the flow appears to be turbulent owing to mixing of the fluid. Conduction along the vertical connecting walls serves to inhibit longitudinal motion by thermally stratifying the fluid.

Predicted flow and temperature fields

Figure 15 shows the predicted isotherms and the velocity vectors for a Rayleigh number $Ra^* = 10^6$. Near the adiabatic vertical outside walls, the temperature decreased almost linearly with the distance from the hot bottom to the cold top horizontal wall. However, natural convection causes the fluid to take up a nonlinear temperature profile at the solid–fluid interface (figure 15*a*). Because of the heating at the bottom of the outside horizontal boundary, the warm fluid rises along part of the vertical wall but does not reach the upper wall. The fluid is cooled at the upper

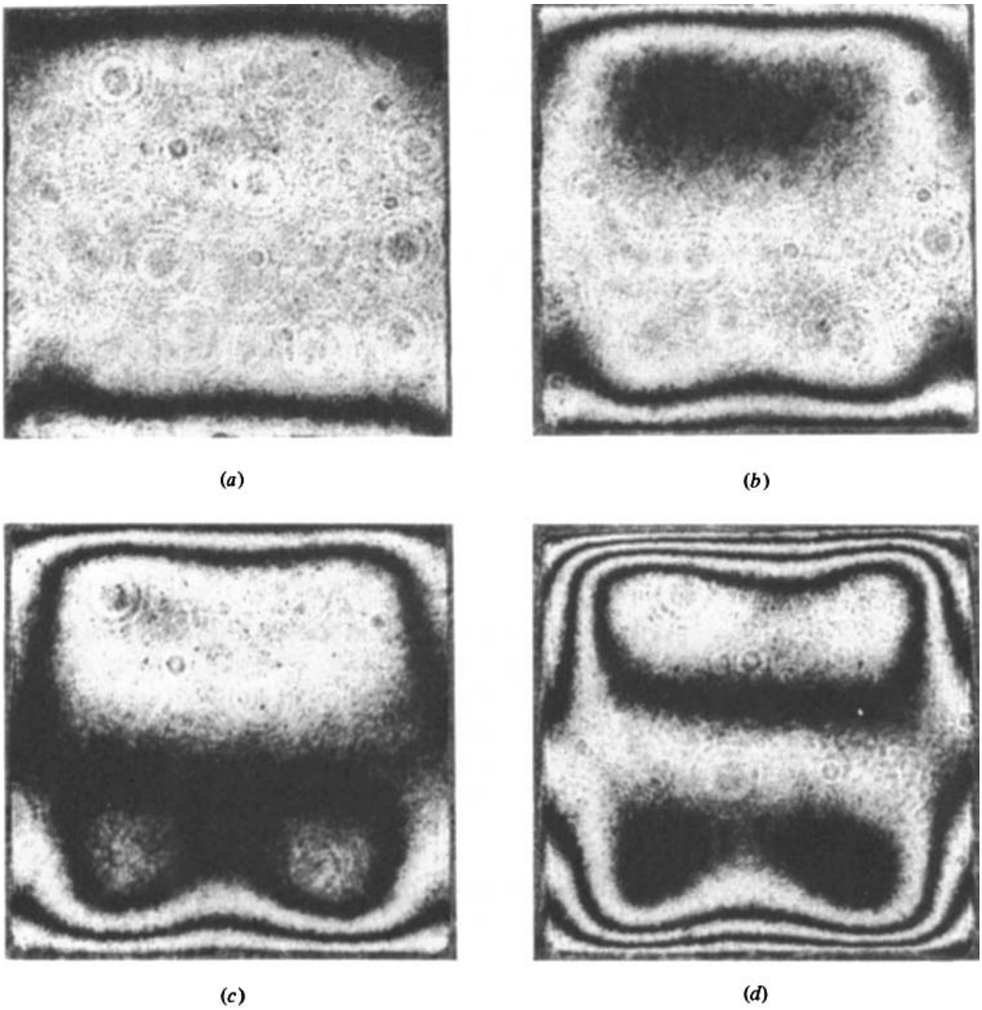

FIGURE 14. Transient isotherms for $Ra^* = 1.01 \times 10^6$, $Pr = 0.71$, $A = 1$, $H/L = 1$, $\phi = 0.36$, $k^* = 7.4$ and $\alpha^* = 0.008$: (*a*) $\tau = 5$; (*b*) 10; (*c*) 20; (*d*) ∞ (steady state).

wall and descends along most of the vertical walls. The thermal structure in the cavity could be explained more clearly by referring to the velocity vectors (figure 15*d*). The air rises from below in the centre of the cavity owing to heating, and reaches the upper cooled wall. It falls down along the vertical walls, which are cooled from the top. However, as the cold air meets the hot air rising along the lower part of the vertical walls, it changes its direction and turns toward the centre of the cavity. Secondary flow predicted in the two corners near the bottom (figure 15*b*) is generated by local temperature differences between the wall and the fluid.

The steady-state local Nusselt numbers at the four walls of the cavity are shown in figure 16. Heating from below is an inherently unstable fluid configuration. Positive Nusselt numbers at the vertical connecting walls in the lower part of the cavity indicate heat addition to the fluid in the lower third of the cavity. The direction of heat transfer at the connecting walls is reversed, and the fluid is cooled in the next $\frac{3}{5}$ of the cavity height. The direction of heat flow is again reversed in the vicinity of

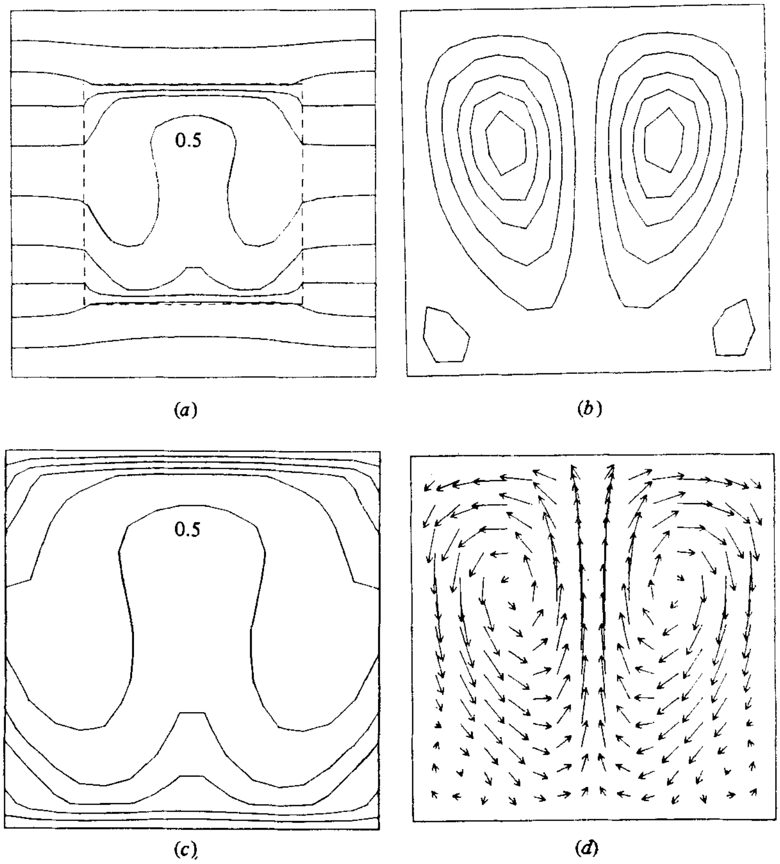

(*a*) (*b*)

(*c*) (*d*)

FIGURE 15. The contours of (*a*) isotherms ($\Delta\Theta = 0.1$); (*b*) streamlines, (*c*) isotherms in the cavity ($\Delta\Theta = 0.064$); (*d*) velocity vectors. $Ra^* = 1.01 \times 10^6$, $Pr = 0.71$, $A = 1$, $L/H = 1$, $\phi = 0.36$, $k^* = 7.4$ and $\alpha^* = 0.008$.

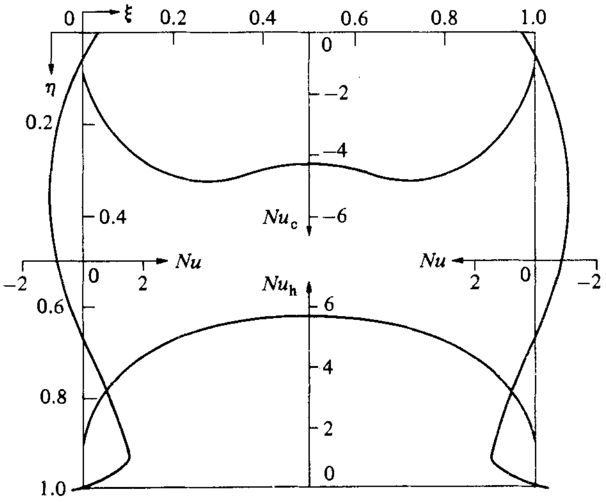

FIGURE 16. Nusselt-number distributions along the four walls of the cavity (see figure 15 for parameters).

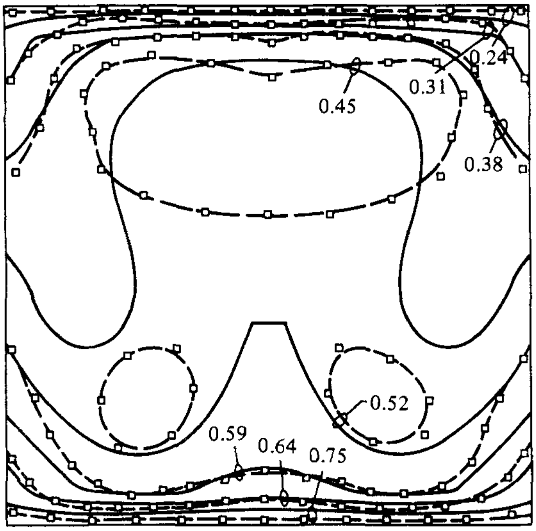

FIGURE 17. Comparison of the measured and predicted steady-state temperatures in air in the absence of radiation; $Ra^* = 1.01 \times 10^6$, $Pr = 0.71$, $A = 1$, $H/L = 1$, $\phi = 0.36$, $k^* = 7.4$ and $\alpha^* = 0.008$.

the cold surface of the cavity and becomes positive over the upper $\frac{1}{10}$ of the connecting walls. Because of the orientation of the enclosure with respect to the gravitational field, the local Nusselt numbers are not symmetrical about the horizontal midplane of the cavity, but are symmetrical about the vertical centreplane of the cavity. The vertical connecting walls have a stabilizing effect on the fluid, and as a consequence the average Nusselt number at the cooled upper horizontal surface is lower than at the heated bottom surface.

Comparison of predictions and experimental data

Figure 17 shows a comparison between the steady-state measured and the predicted steady-state isotherms in the cavity for a typical experiment. The squares indicate the experimental data points and the solid lines denote numerical predictions. Although the trends between data and the predictions are consistent, significant discrepancy is evident at isotherms 0.45 and 0.52. The discrepancy could be due to numerical truncation errors and/or heat losses to the ambient. The model simulates laminar convection, but the thermal-plume activity in the experiments may have produced turbulent convection. Hence the numerical model for laminar flow may not simulate correctly the flow regime at higher Rayleigh numbers.

A comparison between the measured and the predicted solid temperature shows excellent agreement (Kim 1983). This may be due in part to small temperature differences between the horizontal walls and the fact that the solid temperatures are more forgiving and provide a less critical measure of comparison. Similarly, good agreement between data and predictions has been obtained for other experiments with larger temperature differences imposed across the wall. However, the discrepancy between data and predictions was somewhat higher, but still very reasonable.

5. Conclusions

The experiments performed have shown a very significant effect of wall conduction on the convective heat transfer in an enclosure of aspect ratio unity. The effect is greatest for heating from above, and less significant but nonetheless important for heating from the side and the bottom. Wall conduction induces convection in the first, and convection induces conduction in the latter two configurations. Heat conduction along the conducting adiabatic (on the outside) walls simultaneously stabilize and destabilize the fluid in the cavity.

In conjugate heat-transfer problems of the type considered in this study, the heat-transfer-coefficient concept may not be meaningful for correlating analytical and experimental results. The Nusselt number depends not only on the flow but also on the thermal and geometrical parameters of the walls enclosing the cavity.

The experimental data for the particular system considered in the study is in good agreement with the prediction. However, significant studies remain to be done, such as the determination of the velocity field within the enclosure, including measurements of the effect of wall conductance on the convective-flow patterns and heat transfer in relatively small aspect ratio enclosures for different Prandtl number fluids (Catton *et al.* 1983).

REFERENCES

BAJOREK, S. M. & LLOYD, J. R. 1982 Experimental investigation of natural convection in partitioned enclosures. *Trans. ASME C: J. Heat Transfer* **104**, 527–532.

CATTON, I. 1978 Natural convection in enclosure. In *Heat Transfer 1978*, vol. 6, pp. 13–30. National Research Council of Canada.

CATTON, I., AYYASWAMY, P. S. & CLEVER, R. M. 1974 Natural convection flow in a finite, rectangular slot arbitrarily oriented with respect to the gravity vector. *Intl J. Heat Mass Transfer* **17**, 173–184.

CATTON, I., BEJAN, A., GREIF, R. & HOLLANDS, K. G. T. 1983 Natural convection in enclosures. In *Proc. Workshop on Natural Convection* (ed. K. T. Yang & J. R. Lloyd), pp. 24–35. University of Notre Dame.

CHU, T. Y. & GOLDSTEIN, R. J. 1973 Turbulent convection in a horizontal layer of water. *J. Fluid Mech.* **60**, 141–159.

DE VAHL DAVIS, G. & JONES, I. P. 1983 Natural convection in a square cavity, a comparison exercise. *Intl J. Numer. Meth. Fluids* **3**, 227–248.

ELSHERBINY, S. M., HOLLANDS, K. G. T. & RAITHBY, G. D. 1982 Effect of thermal boundary conditions on natural convection in vertical and inclined air layer. *Trans. ASME C: J. Heat Transfer* **104**, 515–520.

HAUF, W. & GRIGULL, U. 1970 Optical methods in heat transfer. In *Advances in Heat Transfer* (ed. J. P. Hartnett & T. F. Irvine), vol. 6, pp. 191–362. Academic.

KIM, D. M. 1983 Heat transfer by combined wall heat conduction, convection and radiation through a solid with a cavity. Ph.D. thesis, Purdue University, West Lafayette, Indiana.

KOUTSOHERAS, W. & CHARTERS, W. W. S. 1977 Natural convection phenomena in inclined cells with finite side-walls – a numerical solution. *Solar Energy* **19**, 433–438.

KRANE, R. J. & JESSE, J. 1983 Some detailed field measurements for a natural convection flow in a vertical square enclosure. In *Proc. ASME/JSME Joint Thermal Engng Conf.* (ed. Y. Mori and W.-J. Yang), vol. 1, pp. 323–329. ASME.

LARSON, D. W. & VISKANTA, R. 1976 Transient combined laminar free convection and radiation in a rectangular enclosure. *J. Fluid Mech.* **78**, 68–85.

MEYER, B. A., MITCHELL, J. W. & EL-WAKIL, M. M. 1982 The effect of thermal wall properties on natural convection in inclined rectangular cells. *Trans. ASME C: J. Heat Transfer* **104**, 111–117.

Ostrach, S. 1978 Natural convection heat transfer in cavities and cells. In *Heat Transfer 1982* (ed. U. Grigull *et al.*), vol. 7, pp. 365–379. Hemisphere.

Peaceman, D. W. & Rachford, H. H. 1955 The numerical solution of parabolic and elliptic differential equations. *J. Indust. Appl. Maths* **3**, 28–41.

Roux, B., Grodin, J. C., Bontoux, P. & Gilly, B. 1978 On a high-order accurate method for the numerical study of natural convection in a vertical square cavity. *Numer. Heat Transfer* **1**, 331–349.

Shiralkar, G. S. & Tien, C. L. 1982 A numerical study of the effect of a vertical temperature difference imposed on a horizontal enclosure. *Numer. Heat Transfer* **5**, 185–197.

Stedfeld, R. 1979 *Materials Engineering/Materials Selector.* Penton/IPC Publications.